

# Another mode in dynamical friction: why does a constant density structure suppress dynamical friction?

Shigeki Inoue<sup>1\*</sup>

<sup>1</sup>*Astronomical Institute, Tohoku University, Sendai 980-8578, Japan*

2009 October 9

## ABSTRACT

Dynamical friction is a fundamental and important phenomenon in astrophysics. The Chandrasekhar formula is a well-known analytical estimation of the effect. However, current astrophysicists have realized that the formula is not correct in some cases because of several approximations dared in the formulation and/or complex non-linearities in the real universe. For example, it has been indicated that the dynamical friction doesn't work in cored density profiles (constant density in the central region) despite that the Chandrasekhar formula predicts drag force even in the constant densities. In the former half of this paper, I discuss by N-body simulations that there are generally two modes in actual dynamical friction. The first mode is the orthodox dynamical friction embodied by Chandrasekhar. The second is another dynamical friction, which is caused by a very small number of field particles resonating with the perturber. The contribution from the resonant particles accounts for a non-negligible fraction of the actual dynamical friction. In the latter half, I discuss why the cored profiles suppress the dynamical friction. One possible explanation is that the second mode drives orbital motion of the perturber as a positive energy feedback source.

**Key words:** methods: N-body simulations – galaxies: dwarf – galaxies: haloes – galaxies: kinematics and dynamics – galaxies: star clusters.

## 1 INTRODUCTION

Dynamical friction (hereafter, DF) is a very important physical process for a wide variety of dynamics, e.g. stellar dynamics, galaxy formation, binary black holes and planetary formation etc. That's why it is in great demand to seek deeper understanding of the nature of DF. As a historical milestone, Chandrasekhar (1943) has succeeded in formulation of the effect of DF. However, several approximations were unavoidable in the derivation of the formula. Moreover, dynamics in the real universe may take a non-linear nature under some circumstances. By efforts of many numerical studies, current astrophysicists have realized that the Chandrasekhar formula is not perfect and loses accuracy of the estimation in some cases (e.g. Tremaine & Weinberg 1984; Jiang & Binney 2000; Fujii et al. 2006).

In this paper, I concentrate on the suppression of DF on a globular cluster (hereafter, GC) in a cored halo of dwarf galaxies (Hernandez & Gilmore 1998; Goerdt et al. 2006; Sánchez-Salcedo et al. 2006; Read et al. 2006; Angus & Diaferio 2009; Cowsik et al. 2009; Inoue 2009). But, the discussion in this paper can be generalized to other astronomical bodies by scaling physical units.

The drag force by DF is negligibly weak for GCs in large systems, like our Galaxy. In contrast, in small systems like dwarf galaxies, the drag force is far too strong (see Binny & Tremaine 2008, chap. 8). Thus, the GCs in dwarfs are presumed to lose their orbital energy and fall into the galactic centre by strong friction force in time-scale of the order of  $\sim 1$  Gyr (Tremaine 1976; Hernandez & Gilmore 1998; Oh et al. 2000; Vesperini 2000, 2001; Goerdt et al. 2006; Bekki 2009). Nevertheless, these GCs still do exist in many dwarf galaxies even now and are as old as the age of universe (e.g. Durrell et al. 1996; Miller et al. 1998; Buonanno et al. 1998, 1999; Strader et al. 2003; Mackey & Gilmore 2003; Lotz et al. 2004; Greco et al. 2007). This problem is referred to as '*the dynamical friction problem*'.

However, a solution of the problem has been proposed. If dwarf galaxies have a cored dark matter halo which has a constant density region in its centre, the DF against the halo is weakened considerably, and GCs should be able to survive beyond the age of the universe. By an analytical approach using the Chandrasekhar formula, Hernandez & Gilmore (1998) discovered that a King-model halo can weaken the DF in the core region. Recently, by N-body simulations, Goerdt et al. (2006), Read et al. (2006) and Inoue (2009) confirmed complete cessation of DF in a core region of haloes. Thus, although the Chandrasekhar formula indicates

\* E-mail:inoue@astr.tohoku.ac.jp

gradual shrinkage of the GC orbit, the N-body simulations demonstrate complete defunctionalization of DF. This discrepancy between analytic and numerical studies (the Chandrasekhar formula and N-body simulations) still remains. Besides, the cessation of DF is a topic not restricted to dwarf galaxies and GCs. Gualandris & Merritt (2008) have discussed the same core-stalling of DF on binary black hole against a cored stellar cluster and suggested that fluctuation of the halo potential weakens the DF in the core.

My goals in this paper are to clarify hidden physics in the nature of DF and the mechanism of the DF suppression in cored density profiles by N-body simulations. It has been known for a long time that DF shows curious behaviors in constant densities. Tremaine & Weinberg (1984) analytically argued that a constant density core causes energy feedback on a perturber by dynamical resonance in positive or negative sense depending on the density distribution. Constant density distribution is called, in other words, ‘harmonic oscillator potential’, which means that all particles in the potential have the same orbital period. In this sense, harmonic potentials are expected to induce resonance effect tremendously and be beyond the applicable domain of the Chandrasekhar formula.

By the way, the cored dark haloes are inconsistent with results of cosmological N-body simulations (e.g. Navarro et al. 1997; Springel et al. 2008). However, among small scale galaxies, many observations of low surface brightness (LSB) galaxies have confirmed the cored dark haloes (e.g. Burkert 1995; Dalcanton & Bernstein 2000; Salucci & Burkert 2000; de Blok et al. 2001; Li & Chen 2009), and nearby dwarf galaxies also favor the cored haloes (Gilmore et al. 2007). In addition, cosmological simulations including baryonic physics also predict core creation by bursty supernovae in the centre of dwarf haloes (Mashchenko et al. 2008; Governato et al. 2009).

This paper is organized as follows: I will explain my simulation method and present my simulation results in §2. In §3, I will show analyses of the data generated by my simulations. In §4, I will summarize my results and present discussion.

## 2 THE SIMULATIONS

My numerical simulation is a typical pure N-body simulation (no gas component). I use Barnes-Hut modified tree-code (Barnes & Hut 1986; Barnes 1990), setting an open angle of  $\theta = 0.5$ . A special-purpose calculator for collisionless N-body simulations, GRAPE-7, is used with the tree algorithm (Makino 1991). The leapfrog time-integrator is adopted with the shared-timestep method. The total number of timesteps is 11841 for the whole of a simulated period which corresponds to 10 Gyrs in the real time-scale.

### 2.1 The settings

In this paper, I use Burkert profile (Burkert 1995) as a cored halo model of dwarf galaxies, which is motivated from observations of LSB galaxies (Salucci & Burkert 2000; Li & Chen 2009) and numerical simulations of formation of dwarf galaxies (Mashchenko et al. 2006),

$$\rho(r) = \frac{\rho_0 r_0^3}{(r + r_0)(r^2 + r_0^2)} \quad ; \quad r < r_{vir} \quad (1)$$

$\rho_0$  is the effective core density,  $r_0$  is the core radius which defines the constant density region. In my simulation, I set  $\rho_0 = 0.1M_\odot/\text{pc}^3$ ,  $r_0 = 1.0$  kpc, and the virial mass of the halo  $M_{vir} \equiv M(r_{vir}) = 2.0 \times 10^9 M_\odot$ , the virial radius  $r_{vir} = 9.88$  kpc. Eq.1 estimates the mass enclosed inside 300 pc to be  $M(300\text{pc}) = 8.79 \times 10^6 M_\odot$ . This value is consistent with the result of Strigari et al. (2008) which has suggested that all dwarfs have the same mass scale,  $M(300\text{pc}) \sim 10^7 M_\odot$ . I add an exponentially decaying envelope to prevent instability at the outer region caused by the artificial cut-off radius,  $r_{vir}$  (Springel & White 1999),

$$\rho(r) = \rho(r_{vir}) \left( \frac{r}{r_{vir}} \right)^a \exp \frac{r_{vir} - r}{r_{decay}}, \quad ; \quad r > r_{vir} \quad (2)$$

where

$$\begin{aligned} a &= c + r \frac{d}{dr} \ln \rho \Big|_{r_{vir}} \\ &= c - \frac{c}{1+c} - \frac{2c^2}{c^2+1}, \end{aligned}$$

and  $c \equiv r_{vir}/r_0$ . I set  $r_{decay} \equiv 0.1r_{vir}$ . With this envelope, total halo mass enclosed in  $r_{cutoff} = 3.16 \times 10^4$  pc becomes  $M_{total} = 2.44 \times 10^9 M_\odot$ .

Velocity dispersion is given by the solution of Jeans equations,

$$\sigma_r^2(r) = \frac{1}{r^{2\beta} \rho(r)} \int_r^\infty dr' r'^{2\beta} \rho(r') \frac{d\Phi}{dr'}, \quad (3)$$

where  $\beta$  is the anisotropy parameter. In this paper, I assume the isotropic velocity state in the halo, setting  $\beta = 0$  ( $\sigma_r = \sigma_\theta = \sigma_\phi$ ). The velocity distribution is determined by local Maxwellian approximation,

$$F(v) = 4\pi \left( \frac{1}{2\pi\sigma^2} \right)^{3/2} v^2 \exp \left( -\frac{v^2}{2\sigma^2} \right), \quad (4)$$

where  $F(v)$  is a probability distribution function of velocities (Hernquist 1993). By the assumptions of isotropic and Maxwellian velocity distribution, I satisfy the suppositions underlying the derivation of the Chandrasekhar formula.

I conduct N-body simulations by  $10^7$  particles to resolve the halo. All halo particles have the same mass,  $m = 2.44 \times 10^2 M_\odot$ , with a softening length of  $\epsilon = 3.0$  pc. Before operating actual simulations, the halo model needs to be relaxed to some extent. I run a simulation without GCs for 2 Gyrs. After the relaxation, I employ the relaxed halo as the initial state ( $t = 0$ ) of the halo.

In my simulation, the GC is represented by a point mass with  $m_{gc} = 2.0 \times 10^5 M_\odot$ . The softening length of the GC particle is set to  $\epsilon_{gc} = 10$  pc. Initial orbital radius of the GC is set to 750 pc. The initial orbit is circular, and I employ a single GC in my simulation. Multi-GC cases are also interesting, but have been investigated by Goerdt et al. (2006), and Inoue (2009), which didn't indicate any large differences from the single GC cases. If the GC is resolved by many particles, some additional effects may play important roles: mass-loss, dynamical heating, etc (e.g. Fujii et al. 2006; Miocchi et al. 2006; Esquivel & Fuchs 2007; Capuzzo-Dolcetta & Miocchi 2008). Besides, stellar components in a dwarf galaxy can enhance the DF of GCs (Sánchez-Salcedo et al. 2006; Bekki 2009). However, in

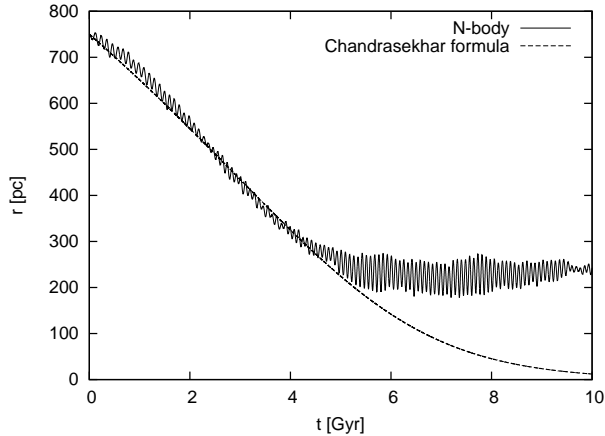


**Figure 1.** The time-evolutions of orbital radius of the GC. The Chandrasekhar formula is calculated with  $\ln \Lambda = 3.72$ .

this paper, I concentrate on investigations of fundamental physics of DF, and do not consider such effects.

I calculate the orbit of the GC in the cored dwarf halo by executing the N-body simulation. The simulation outputs 3-dimensional positions and velocities of all field particles at 0.5 Gyr intervals for the analyses in §3.

## 2.2 The results

The time-evolution of orbital radius of the GC is plotted in Fig.1. As a comparison, I also plot an analytic calculation by the Chandrasekhar formula,

$$\frac{dv_c}{dt} = -\frac{4\pi \ln \Lambda G^2 \rho m_{gc}}{v_c^2} \left[ \text{erf}(X) - \frac{2X}{\sqrt{\pi}} e^{-X^2} \right], \quad (5)$$

$$\frac{dr}{dt} = \frac{r}{v_c} \frac{dv_c}{dt}, \quad (6)$$

where  $X \equiv v_c/(\sqrt{2}\sigma)$ .  $v_c$  is circular velocity of the GC as a function of radius.  $G$  is the gravitational constant. For the Coulomb logarithm, I set  $\ln \Lambda = 3.72$ , which is determined by the best-fitting to the result of simulation for  $t < 4$  Gyr. But, if I take the original definition,  $\ln \Lambda \equiv \ln(b_{max}/b_{min}) = \ln(r_0/\epsilon) = 5.81$ , where  $b_{max, min}$  are the maximum and the minimum impact parameter. In the derivation of Eq.6, the assumption of circular orbits is used (Hernandez & Gilmore 1998; Inoue 2009; Cowsik et al. 2009). As seen from Fig.1, in the N-body simulation, the orbital shrinkage stops after the GC entered into the constant density region ( $r \lesssim 300 pc$ ). On the other hand, the Chandrasekhar formula fails to reproduce the N-body result in the core region, in spite of the excellent fit outside the core. The same results have been indicated by Goerdts et al. (2006), Read et al. (2006) and Inoue (2009). In this paper, I define  $t \lesssim 5$  Gyr as ‘*exerting DF phase*’, and  $t \gtrsim 5$  Gyr as ‘*suppressed DF phase*’.

The density profiles of the halo are plotted in Fig.2. Even in the end-state of the simulation, the density profile is stable. The energy conservation rate of the system,  $1 - E_{end}/E_{ini}$ , is  $1.92 \times 10^{-4}$ .

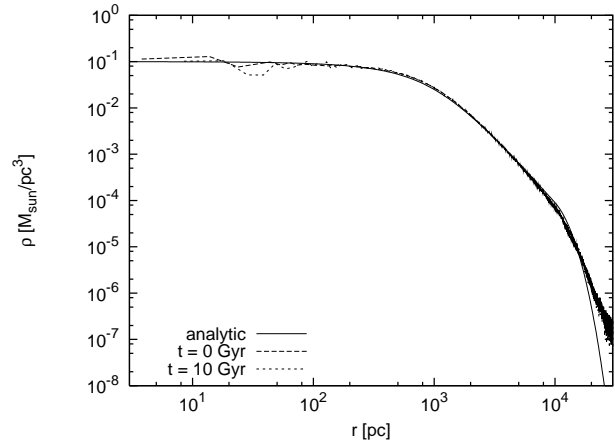


**Figure 2.** Density profiles of field particles of analytic model (Eq.1 and 2) and in the N-body simulation for  $t=0$  and 10 Gyr.

## 3 THE ANALYSIS

In this section, I analyze dynamical state of the field particles. The Chandrasekhar formula has been derived under the assumption of isotropic velocity field. Moreover, interaction between a perturber and field particles is supposed to be integration of countless two-body interactions and orbital periodicity of all particles is not taken into account. On the other hand, actual N-body systems consist of mutually interacting particles. The motions of particles are periodic orbits under the potential field.

In the following subsections, I will show in details orbital motions of the field particles and their influences on the perturber. Besides, I will discuss that these behaviors are different between the exerting and suppressed DF phase.

### 3.1 The exerting DF phase

In the N-body simulation, for  $t < 5$  Gyr, DF is clearly exerted on the GC, leading to orbital shrinkage. The Chandrasekhar formula with  $\ln \Lambda = 3.72$  succeeds in estimation of the effect in this phase.

Firstly, to investigate the dynamical state of the field particles, I calculate dynamical energies of all particles. The specific energy of the  $i$ th particle can be estimated by

$$E_i = \frac{v_i^2}{2} - \frac{Gm_{gc}}{\sqrt{|x_{gc}^{\vec{}} - \vec{x}_i|^2 + \epsilon_{gc}^2}} - \sum_{\substack{j=1 \\ j \neq i}}^n \frac{Gm}{\sqrt{|\vec{x}_j - \vec{x}_i|^2 + \epsilon^2}}, \quad (7)$$

where  $\vec{x}_{i,j,gc}$  mean position vectors of the  $i, j$ th field particles and the GC, respectively. The sum in the third term is taken over all other field particles.

Next, I calculate increase of  $E_i$  at intervals of 1 Gyrs. In Fig.3, I show a distribution of all field particles in  $E-\Delta E$  diagram.  $\Delta E$  corresponds to the increase of  $E_i$  between 2 and 3 Gyr. In this figure, I can find a notable feature. At a certain energy,  $-\log |E/\Phi_0| \simeq -0.05$ , there are some particles of which energies changed largely. This feature looks like two *horns*. Thus, I define  $-\log |E/\Phi_0| < -5.23 \times 10^{-3}$  and  $\Delta E/\Phi_0 > 1.27 \times 10^{-2}$  (inside the red square) as *positive-horn* (P-horn),  $-\log |E/\Phi_0| < -5.23 \times 10^{-3}$  and  $\Delta E/\Phi_0 < -1.27 \times 10^{-2}$  (inside the green square) as *negative-horn* (N-horn). The numbers of P- and N-horn particles

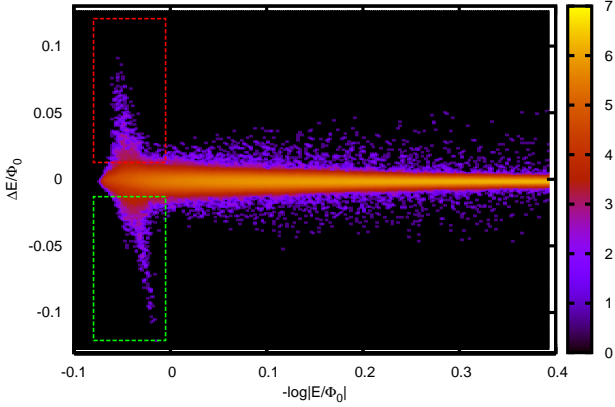


**Figure 3.** Contour plot of distribution of field particles in a  $E - \Delta E$  diagram. The vertical axis,  $\Delta E$ , means an amount of increase of dynamical energy of each particle between 2 and 3 Gyr:  $\Delta E \equiv E(3\text{Gyr}) - E(2\text{Gyr})$ . The horizontal axis indicates energy before the change:  $E(2\text{Gyr})$ . The values are normalized by  $\Phi_0$  which is the potential energy at  $r = r_0$  estimated by Eq.1 and 2. Colour-bar labels mass in a bin,  $\log(M/M_\odot)$ . Black colour means no mass. In this diagram, I separate the particles into three groups; positive-horn (the red square), negative-horn (the green square), the others.

in this plot are 1,513 ( $3.69 \times 10^5 M_\odot$  in total) and 2,028 ( $4.95 \times 10^5 M_\odot$  in total), respectively.

In Fig.4, I show 3-dimensional positions of the P- and N-horn particles at  $t=2$  Gyr. In the top panel, the particles are projected on the GC orbital plane. By calculating dot products of angular momentum vectors of the GC and the horn particles, I confirm that most of the particles plotted in Fig.4 have positive dot products at  $t=2$  Gyr: prograde rotations with the GC (1,194 of 1,513 P-horn and 1,734 of 2,028 N-horn particles have prograde rotations). Thus, I find that most of the P-horn particles are rotating behind the GC orbit, whereas, the N-horn particles are orbiting ahead of the GC. The bottom panel shows a edge-on view to the GC orbital plane, which indicates somewhat different distributions; the P-horn particles are more strongly concentrated toward the GC orbital plane than the N-horn particles. In any case, most of these particles have short distances from the GC and the prograde rotations. I can ascribe the horn-feature in Fig.3, the large increase or decrease of energy, to the similarity between orbits of the horn particles and the GC. Since the P- and N-horn particles have similar velocity vectors to the GC, these particles strongly interact with the GC. Conversely, the GC ought to be affected by these particles. To give a expediential name, hereafter, I call both of the P- and N- horn particles *resonant* particles.

I examine orbital motions of the resonant particles. In Fig.5, I illustrate typical orbits of the P- and N-horn particles in the coordinate rotating with the GC. The P-horn particle in this figure approaches the GC from behind. The orbit expands when catching-up, and finally retreats from the GC after the orbital expansion. This orbital expansion corresponds to the energy increase seen in Fig.3. On the other hand, the N-horn particle orbit is the reverse, comes close to the GC (in inertia coordinate, the GC is catching up to the N-horn particle), shrinks the orbital radius, and runs away from the GC. As a result, the energy of N-horn par-

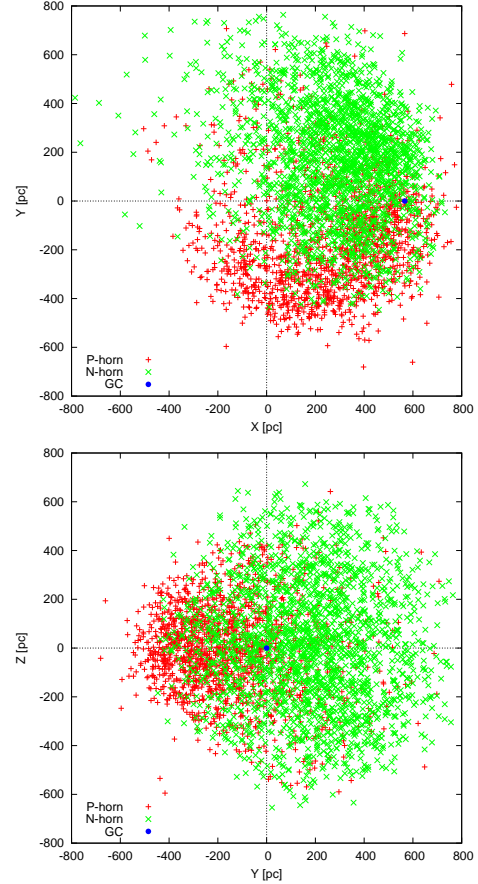


**Figure 4.** Positions of the P-, N-horn particles and the GC at  $t = 2$  Gyr. By coordinate exchange, I set X-axis to the direction of the GC from the galactic centre. Z-axis coincides with the GC angular momentum vector. Y-axis lies in the GC orbital plane. The GC is rotating counter-clockwise in the X-Y plane.

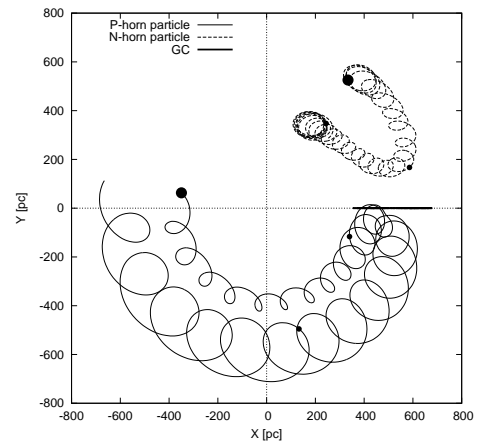


**Figure 5.** Examples of typical orbits of the P- and N-horn particle in rotating coordinate with the GC. Although the resonant particles are defined by energy increase in  $t=2-3$  Gyr, the orbits plotted here are for  $t=1-4$  Gyr. The coordinate system is rotating counter-clockwise. The large (small) dots indicate positions of the particles at  $t=1$  Gyr ( $t=2$  and  $t=3$  Gyr).

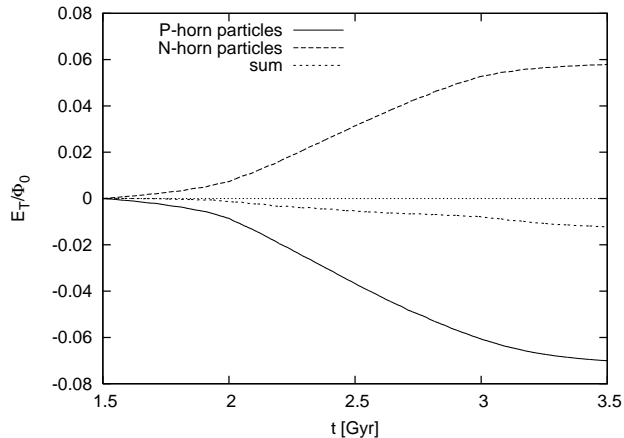


**Figure 6.** Cumulative energy transfers to the GC from the P- and N-horn particles. The short-dashed line corresponds to the sum of both. Increase in  $E_T$  means energy injection into the GC, decrease means energy absorption from the GC.

ticle decreases. The mechanism of these orbital behaviors is simple. Under density gradients, generally, inner orbits have shorter orbital periods and outer orbits have longer periods. The P-horn particle is pulled forward by gravity of the GC, and gains energy. But, this energy increase causes the orbital expansion and makes angular velocity slow. In the case of the N-horn particle, the particle is pulled backward and decrease the energy. This energy decrease results in the orbital shrinkage and faster angular velocity. This phenomenon, that the particle slows down in azimuth when pulled forward and speeds up when held back, has come to be called ‘the donkey effect’ (Lynden-Bell & Kalnajs 1972; Binny & Tremaine 2008). The orbits in Fig.5 imply that higher energy particles lose the energy and lower energy particles gain the energy. This behavior can be confirmed in Fig.3, which indicates that the two horns lean slightly from top-left to bottom-right. Moreover, Fig.5 implies that these orbits cannot get across the GC orbit on Y-axis; the P- and N-horn particles don’t interchange with each other. Fujii et al. (2009) have also investigated orbits of resonant particles in 1:1 mean motion resonance (Trojan horseshoe orbits) which look like the orbits in Fig.5 (see Fujii et al. 2009, Fig.7). It is worthy of special mention that these orbits exhibit quite different behavior from two-body interaction that is assumed in the derivation of the Chandrasekhar formula.

To probe the energy transfer from the resonant particles to the GC, I rerun the same simulation while calculating

$$E_T(t) = \int_{t_{ini}}^t v_{gc}^{\vec{}}(t') \cdot \vec{a}_{spc}(t') dt'. \quad (8)$$

This integration means cumulation of the integrand on each timestep.  $\vec{a}_{spc}$  represents net acceleration exerted on the GC by a specific particle group (e.g. the P-, N-horn or the other particles).

By this equation, I compute the energy transfers to the GC in the simulation and show the result in Fig.6. Though the horn particles were defined by energy change during 2-3 Gyr, I draw the energy transfers during  $t=1.5-3.5$  Gyr in Fig.6; setting  $t_{ini} = 1.5$  Gyr in Eq.8. In agreement with a naive expectation, I find that the P-horn particles absorb

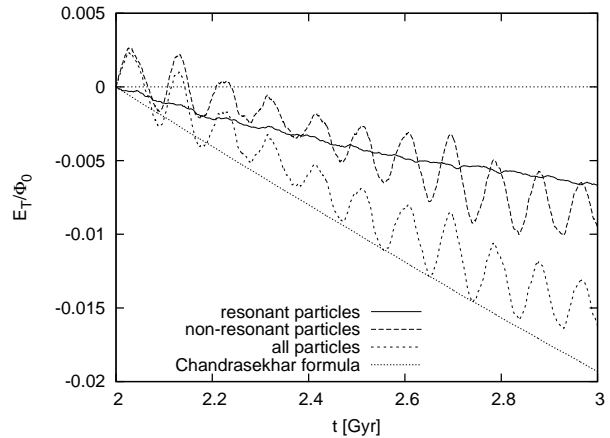


**Figure 7.** Comparison of cumulative energy transfers to the GC. The solid line labelled as ‘resonant particles’ is the same as the result of ‘sum’ in Fig.6 but setting  $t_{ini} = 2$  Gyr in Eq.8.

energy from the GC and the N-horn particles inject energy into the GC. It is notable that the behaviors of the injection and absorption are monotonic. The transfers are sharp in 2-3 Gyr, slow in  $t \lesssim 2$  Gyr and  $t \gtrsim 3$  Gyr. This implies that the transfers are transient.

The energy transfers in Fig.6 don’t completely balance; however, the energy absorption by the P-horn particles slightly surpasses the injection by the N-horn. I compare the energy transfer by the resonant particles with that by the other particles, non-resonant particles. The comparison is shown in Fig.7. For  $t=2-3$  Gyr in which the P- and N-horn particles are under the resonance with the GC, the non-resonant particles also steal energy from the GC. This decrease in the GC energy seems to be caused by DF against the non-resonant field particles. Interestingly, the energy decrease caused by the resonant particles is comparable to the DF by the non-resonant particles, accounting for a half of actual DF by all particles. The dotted line labelled as ‘Chandrasekhar formula’ is calculated by substituting Eq.5 for  $\vec{a}_{spc}$  in Eq.8 using the data of GC orbit in the simulation. The DF from all particles is well fitted by the Chandrasekhar formula with  $\ln \Lambda = 3.72$ , which has succeeded in reproducing the orbital shrinkage in the exerting DF phase. This result implies that actual DF can be separated into two modes. The first mode is the well-known conventional DF based on the concept of Chandrasekhar (1943). This is a DF that is attributed to random encounters with a myriad of non-resonant particles in an isotropic velocity distribution. On the other hand, unlike the first mode, the cause of the second mode is a small number of resonant particles which have anisotropic velocities; the prograde rotations with the GC. The resonant particles have only 0.0354 per cent of the total mass of the system.

However, the result in Fig.7 doesn’t necessarily means that DF caused by ‘true’ resonant particles accounts for a half of the actual DF. This is because the criterion for defining the resonant particles is somewhat arbitrary. Even in two-body interaction, if a field particle has a similar velocity vector to  $v_{gc}^{\vec{}}$  and a small impact parameter, the particle causes strong interaction and large energy transfer. There would be no clear-cut way to extract only the true resonant

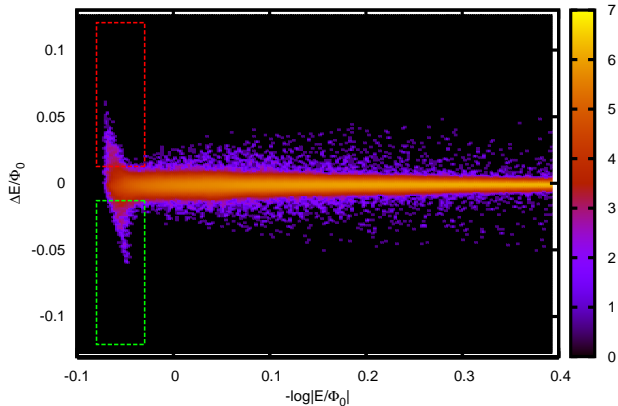


**Figure 8.** The same figure as Fig.3, but the differential is taken between 7 and 8 Gyr:  $\Delta E \equiv E(8\text{Gyr}) - E(7\text{Gyr})$ . Criteria for defining P-horn (N-horn) particles is  $-\log |E/\Phi_0| < -3.0 \times 10^{-2}$  and  $\Delta E/\Phi_0 > 1.27 \times 10^{-2}$  ( $\Delta E/\Phi_0 < -1.27 \times 10^{-2}$ ).

particles. However, it is sure that the resonant particles defined in Fig.3 include many true resonant particles.

### 3.2 The suppressed DF phase

For  $t > 5$  Gyr, the DF doesn't seem to act on the GC to shrink the orbit. This phenomenon itself has already been known. Hernandez & Gilmore (1998) has found that this core-stalling of DF can be explained by the Chandrasekhar formula. However, their estimation was based on the assumption of completely constant density in the core. Without this assumption, the Chandrasekhar formula predicts slow but certain orbital shrinkage (Goerdet et al. 2006; Read et al. 2006; Inoue 2009), as seen in Fig.1.

On the other hand, the N-body simulations indicate the complete suppression of the DF in the cored region. The Chandrasekhar formula is no longer viable in this phase. Read et al. (2006) has suggested that the mechanism of the DF suppression is 'co-rotating state', in which the number of particles rotating prograde with the GC increases in the cored structure. Inoue (2009), however, revealed the co-rotating state to be marginal. Also, Gualandris & Merritt (2008) suggested that fluctuation of the halo potential weakens the DF in the core. But, they supposed the case of a black hole and a stellar cored structure, the perturber being so heavy that their theory is not applicable to the case of a dwarf galaxy and GCs. Thus, the mechanism of the suppressed DF is still controversial.

In this subsection, to seek the true mechanism, I execute the same analyses as in the previous subsection. In Fig.8, I show the  $E$ - $\Delta E$  diagram for 7-8 Gyr and redefine P- and N-horn particles by the same way. The numbers of the P- and N-horn particles are 613 and 834, respectively. Positions of these resonant particles at  $t=7$  Gyr are plotted in Fig.9. As well as the exerting DF phase, I confirm that most of the resonant particles have prograde rotations with the GC (399 of 613 P-horn and 761 of 834 N-horn particles). In the top panel of Fig.9, however, the distribution of the P-horn particles indicates a shorter tail than in Fig.4.

In Fig.10, I illustrate an example of each resonant particle. This figure indicates very complex orbits. Both particles

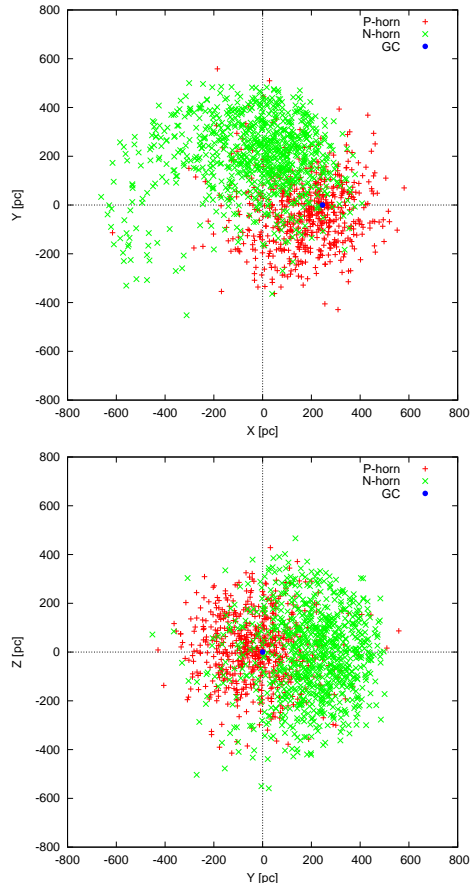


**Figure 9.** Positions of P-, N-horn particles and the GC at  $t = 7$  Gyr. The coordinate system of this plot is determined by the GC angular momentum vector at  $t = 7$  Gyr.

come close to the GC from the front, some inside the GC orbital radius, rotate around the GC, expand the orbits and finally go away behind the GC. It seems as if the particles dodge the GC. Although the two particles are respectively defined as a P- and a N-horn particle, these orbits are identical. This means that the P- and N-horn particles can interchange with each other. Regardless of the complexity, the orbits come to be explainable by considering absence of the donkey effect (see §3.1) in the constant density region. In constant densities, orbital period becomes independent of orbital radius. In coming close to the GC, the particles are orbiting slightly outside the core with slower angular velocities than the GC. But, by the gravity from the GC, the particles are pulled backward and lose energy. The particles sink toward the centre by the energy loss. However, by the absence of the donkey effect in the core, the angular velocities of the particles are constant even in the inner radii. The particles can pass through the GC orbit. After getting behind the GC, the particles are pulled forward by the GC and gain energy. As a result, the orbits of the particles expand again and are exiled from the core. The two particles in Fig.10 rotate with slower angular velocities than the GC (the clockwise motions in the rotating coordinate with the GC). I find that almost all resonant particles rotate in the clockwise direction in the rotating coordinate and have slower angular velocities than the GC. This is because

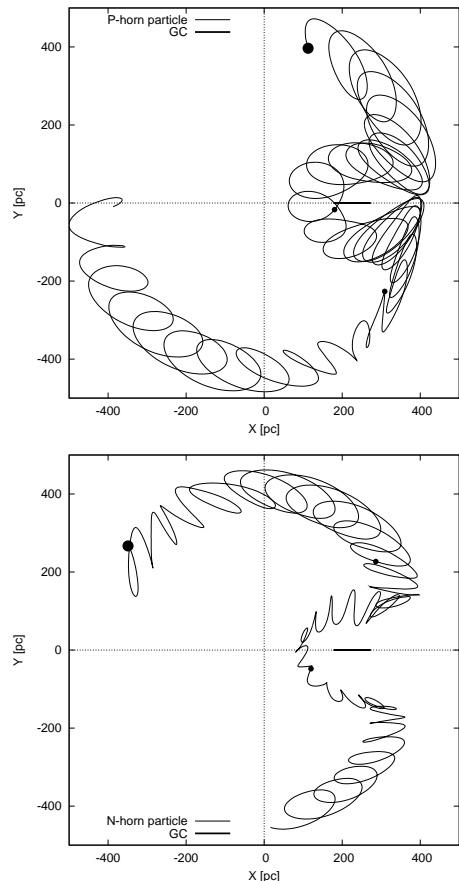


**Figure 10.** Examples of typical orbits of the P- and N-horn particle in the coordinate rotating with the GC. Although the resonant particles are defined by energy increase in  $t=7-8$  Gyr, the orbits plotted here are in  $t=6-9$  Gyr. The large (small) dots indicate positions of the particles at  $t=6$  Gyr ( $t=7$  and  $t=8$  Gyr).

all particles have the same angular velocity in the constant density. There is no particle rotating faster than the GC in the core.

In Fig.11, I show cumulative energy transfers into the GC. In consistency with the complexity of the resonant orbits, the energy transfers into the GC also show very intricate features. The transfers are no longer monotonic, unlike in the exerting DF phase (Fig.6). The N-horn particles continue to inject energy until  $t \sim 8$  Gyr, but absorb energy from the GC afterwards. Meanwhile, the P-horn particles inject a little energy at first, but largely absorb later. Thus, the total transfer from all resonant particles indicates an intricate waving behavior. Although the particles are defined by  $E(8Gyr) - E(7Gyr)$ , the resonant particles largely inject and absorb energy in  $t \lesssim 7$  Gyr and  $t \gtrsim 8$  Gyr. These behaviors implies not transient but long-term resonances on the particles.

From the discussion above, in the suppressed DF phase, it is clear that the resonance on some particles has a long duration. In this case, I couldn't extract all resonant particles successfully. In order to overcome this difficulty, I have to examine the resonance in long-term observations. By the same procedure as in Fig.8, I screen particles in  $t=5-6$ ,  $6-7$ ,  $7-8$ ,  $8-9$ ,  $9-10$  Gyr by calculating  $\Delta E$ . I gather the particles

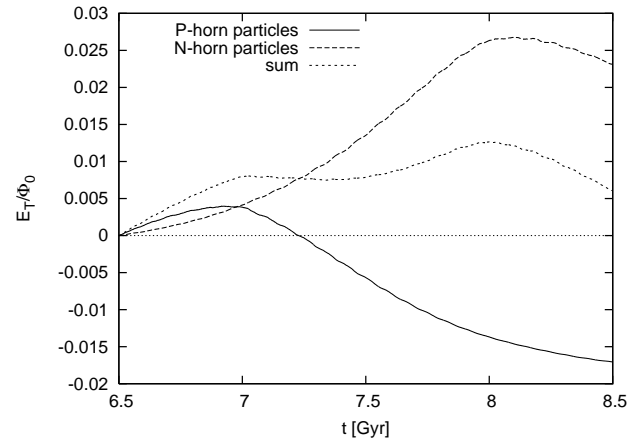


**Figure 11.** Cumulative energy transfers to the GC from the P- and N-horn particles for  $t > t_{ini}$  ( $t_{ini} = 6.5$  Gyr in this plot).

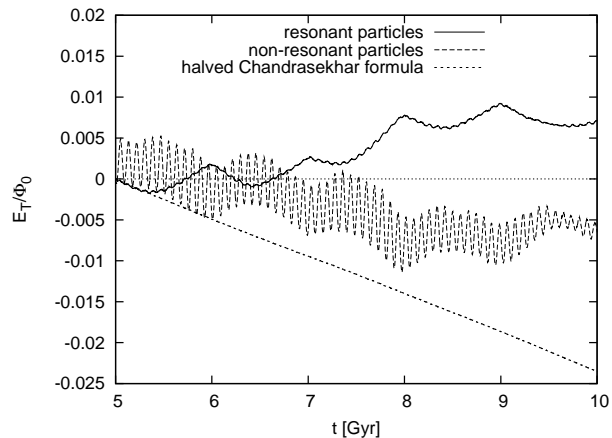
**Table 1.** The numbers of particles defined as resonant particles in each time-intervals. The top and bottom tables are 1Gyr-interval and 0.5Gyr-interval, respectively. The leftmost column indicates time-period in which I calculate  $\Delta E$  to define resonant particles. The bottommost row is the number of particles for which all particles listed above are gathered. Because some particles overlap, the number of particle gathered is not identical to simple sum of rightmost columns.

period	P-horn	N-horn	total
5 - 6 Gyr	590	604	1194
6 - 7 Gyr	772	654	1426
7 - 8 Gyr	613	834	1447
8 - 9 Gyr	861	710	1571
9 - 10 Gyr	929	884	1813
gathered			4787

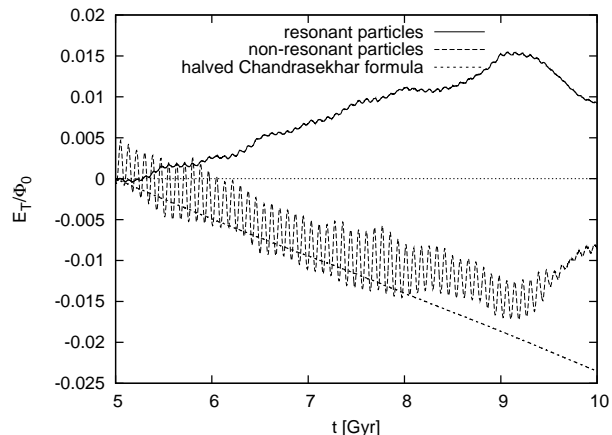
  

period	P-horn	N-horn	total
5 - 5.5 Gyr	195	345	540
5.5 - 6 Gyr	292	251	543
6 - 6.5 Gyr	253	337	590
6.5 - 7 Gyr	460	227	687
7 - 7.5 Gyr	365	462	827
7.5 - 8 Gyr	526	363	889
8 - 8.5 Gyr	977	352	1329
8.5 - 9 Gyr	696	658	1354
9 - 9.5 Gyr	1438	895	2333
9.5 - 10 Gyr	1604	1082	2686
gathered			6776

listed in this five time-periods and get the number of gathered particles listed in the bottommost row of Table 1. The numbers of particles listed up are shown in the top of Table 1. While operating the same simulation starting from  $t=5$  Gyr, I compute energy transfers into the GC from the *gathered* resonant particles and the others by calculating Eq.8; all particles listed in the gathered list are used to calculate in the entire simulated period. The result is shown in Fig.12. In this figure, the cumulative energy transfer from the resonant particles gradually increases. On the other hand, the non-



**Figure 12.** Cumulative energy transfers to the GC from the *gathered* resonant and other, non-resonant, particles in the suppressed DF phase. For comparison, an analytical estimation by the Chandrasekhar formula is also plotted, but it is reduced by half from the naive estimation by Eq.5.



**Figure 13.** The same plot as Fig.12, but using 0.5Gyr-interval to extract the gathered resonant particles.

resonant particles absorb energy from the GC. But, these cumulative transfers indicate periodic flapping. This periodicity appears just in 1 Gyr period, implying an artificial effect caused by setting the time-interval to calculate  $\Delta E$  to be 1 Gyr.

Therefore, I follow the same procedure to calculate  $\Delta E$  with 0.5Gyr-interval. The numbers of particles listed up are shown in the bottom of Table 1. I show cumulative energy transfers in Fig.13 with an analytical estimation by Chandrasekhar formula for the sake of comparison. But the analytical estimation is halved, according to the result of §3.1. The periodic flapping in Fig.12 disappears. Moreover, the energy injection from the resonant particles are monotonic for  $t \lesssim 9$  Gyr. The energy absorption by the non-resonant particles is also monotonic. Interestingly, the halved analytic formula provides excellent fit to the absorption for  $t \lesssim 9$  Gyr though there is a slight deviation at  $t \sim 8$  Gyr. This excellent fit by the halved Chandrasekhar formula means that the DF by the non-resonant particles is not different from in the exerting DF phase, always exerting the same drag force.

But, on the other hand, the behavior of the resonant particles is largely different; the resonant particles continue to inject energy into the GC only in the suppressed DF phase. These energy transfers from the resonant and non-resonant particles are completely opposite. This implies that these influences are canceled out and the GC orbit can remain on a constant orbital radius as if the DF on the GC vanished.

However, for  $t \gtrsim 9$  Gyr, both of energy transfers come to be inverse. But, these unfavorable features doesn't prove defects of my theory. I will explain this inverted behaviors in the following discussion.

### 3.2.1 Why is energy injected from the resonant particles?

The result above demonstrates that the resonant particles inject energy into the GC and cancel out the effect of the DF caused by the non-resonant particles. However, the orbits shown in Fig.10 exhibit both of an orbital shrinkage and an expansion around the GC. Besides, the final orbital radii are almost retrieved to the initial radii eventually. In other words, each resonant particles doesn't necessarily decrease its energy; these doesn't necessarily inject energy into the GC. Notwithstanding, the energy injection is obviously indicated in Fig.13. Right then, why can the resonant particles inject energy? I tackle here to answer this problem. The key issues are order of energy transfers and increasing numbers of the resonant particles.

Concerning the first key, look back to Fig.11. Both of the P- and N-horn particles inject energy before absorb. This means that the energy injection precedes the absorption. The sum of the contributions from the P- and N-horn particles (the short-dashed line) behaves in a similar manner, i.e., the energy injection precedes the absorption. Moreover, in Fig.10, the orbits show sudden orbital shrinkage in the front of the GC. Afterward, the orbits expand again. This may also imply that the energy injection precedes the absorption. As to the second key, Table 1 shows that the resonant particles continue to increase in number as time goes on.

From these two keys, I conclude as follows. Some resonant particles inject energy, which is followed by energy absorption. But, because particles to be resonating later are more numerous than the former, much larger injection is expected. This larger injection exceeds the former absorption. The GC can thus continue to gain energy from the resonant particles. If analogizing with our real lives, *even if you are in debts to 10 persons and have to pay it back, you can keep money by new debts to 20 persons.*

The inverse behavior in Fig.13 can be explained by the same logic. In this figure, I have picked up the resonant particles during  $t=5-10$  Gyr at the intervals of 0.5 Gyr. This means that there is no injection by new particles resonating after  $t = 10$  Gyr. I suggest that, by the lack of new resonant particles, the energy transfer declines at  $t \sim 9$  Gyr. As a proof of this inference, I show Fig.14. I use the particle-lists shown in the bottom of Table 1, but, the particle-lists are cut off at  $t = 9$  Gyr and  $t = 8$  Gyr; using the particles listed for  $t=5-8$ ,  $5-9$ ,  $5-10$  Gyr. In the case of using the particle-lists for  $t < 9$  Gyr and  $t < 8$  Gyr, the inverse behaviors begin at  $t \sim 8$  Gyr and  $t \sim 7$  Gyr, respectively. In all cases, the beginning of the inverse behavior predates the cut-off by  $\sim 1$  Gyr. From this result, I infer that the inverse behavior in Fig.13 is caused by lack of next resonant particles. In



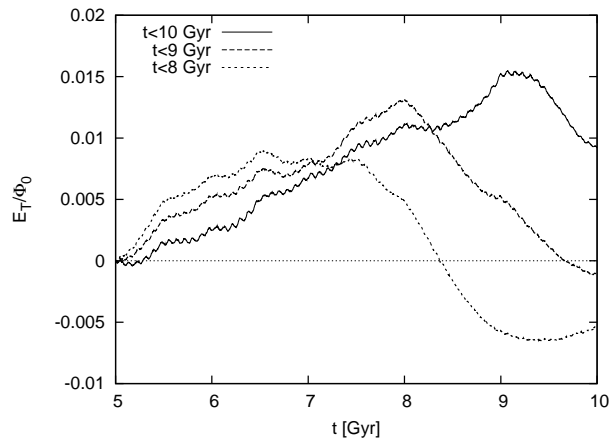


**Figure 14.** Dependence of energy transfers on when the particle-list is cut off. I apply the particle-lists shown in the bottom of Table 1 (0.5Gyr-interval). But, the lists used are all,  $t < 9$  Gyr and  $t < 8$  Gyr.

addition, this result reinforces the theory above; the energy injection arises from the increase of the resonant particles in number.

#### 4 DISCUSSION AND SUMMARY

By the N-body simulation in this paper, I conclude as follows. In the exerting DF phase, the Chandrasekhar DF formula seems good at estimating the actual DF. But, quantitatively, a very small number of particles accounts for a half of the actual DF although they occupy less than 0.1 per cent of the halo mass. These particles include particles resonating with the perturber, which have quite different orbits from two-body interaction those particles experiencing. The presence of such resonant particles disagrees with the concept of Chandrasekhar (1943). But, in his formula, uncertainty of determining  $\ln \Lambda$  would conceal the contribution from the resonant particles.

In the suppressed DF phase, the behavior of the second mode in the DF, the resonant particles, alters direction of energy transfer while the other particles exert DF in the first mode, the orthodox DF, ceaselessly. The resonant particles feed energy into the perturber. As a result, the second mode cancels out the first. The orbit of the perturber is thus stabilized. This is the mechanism of the suppressed DF in a constant density structure.

However, there still appears to be remaining questions. Why do these two modes completely balance with each other? In Fig.12 and 13, the energy transfers seem to balance completely. However, it is still a mystery why quantities of the injection and absorption are always equal. Moreover, why can the resonant particles increase in number? Read et al. (2006) and Inoue (2009) have suggested that the number of prograde rotating particles with a perturber increases in the core region. But, in any collisionless particle systems, phase-space density can never increase. In this paper, I couldn't give concrete answers to these questions.

The result of this paper indicates that the second mode in DF arises from the resonant particles which have anisotropic velocity field, co-rotating orbits and close prox-

imity to the perturber. This property of the second mode implies sensitivity of the actual DF to velocity field of the halo models. I employed in this paper the isotropic assumption,  $\beta = 0.0$  in Eq.3, as the most fundamental model. But, many numerical simulations have suggested dependence of  $\beta$  on radius in dwarf and other galaxies (van Albada 1982; Mashchenko et al. 2008; Binney & Tremaine 2008). These results imply that actual DF against a *live* halo would depend sensitively on the distribution functions of the haloes. In addition, there are some generalised applications of the Chandrasekhar formula; against aspherical distributions (Binney 1977; Pesce et al. 1992), variable  $\ln \Lambda$  (Hashimoto et al. 2003), DF on spherical bodies (Esquivel & Fuchs 2007), in a gaseous medium (e.g. Ostriker 1999; Kim et al. 2008), etc. The results in this paper alert to thoughtless usages of the Chandrasekhar formula.

#### ACKNOWLEDGMENTS

The numerical simulations reported here were carried out on MUV (Mitaka Underground Vineyard) GRAPE systems kindly made available by CfCA (Center for Computational Astrophysics) at National Astronomical Observatory of Japan. The numerical code was based on a software distributed on the website of Joshua E. Barnes (<http://ifa.hawaii.edu/~barnes/software.html>). I thank Masafumi Noguchi for his fascinating and helpful discussion, Masaki Iwasawa for his innovative advice.

#### REFERENCES

- Angus G. W., Diaferio A., 2009, MNRAS, 396, 887
- Barnes J., 1990, J. Comput. Phys., 87, 161
- Barnes J., Hut P., 1986, Nat, 324, 446
- Bekki K., 2009, preprint (astro-ph/0911.5461)
- Binney J., 1977, MNRAS, 181, 735
- Binney J., Tremaine S., 2008, Galactic Dynamics Second Edition. Princeton Univ. Press, Princeton
- Buonanno R., Corsi C. E., Castellani M., Marconi G., Pecci F. F., Zinn R., 1999, AJ, 118, 1671
- Buonanno R., Corsi C. E., Zinn R., Pecci F. F., Hardy E., Suntzeff N. B., 1998, ApJ, 501, 33
- Burkert A., 1995, ApJ, 447, 25
- Capuzzo-Dolcetta R., Miocchi P., 2008, ApJ, 681, 1136
- Chandrasekhar S., 1943, ApJ, 97, 255
- Cowsik R., Wagoner K., Berti E., Sircar A., 2009, ApJ, 699, 1389
- Dalcanton J. J., Bernstein R. A., 2000, AJ, 120, 203
- de Blok W. J. G., McGaugh S. S., Bosma A., Rubin V. C., 2001, ApJ, 552, 23
- Durrell P. R., Harris W. E., Geisler D., Pudritz R. E., 1996, AJ, 112, 972
- Esquivel O., Fuchs B., 2007, MNRAS, 378, 1191
- Fujii M., Funato Y., Makino J., 2006, PASJ, 58, 743
- Fujii M., Iwasawa M., Funato Y., Makino J., 2009, ApJ, 695, 1421
- Gilmore G., Wilkinson M. I., Wyse R. F. G., Kleyna J. T., Koch A., Evans N. W., Grebel E. K., 2007, ApJ, 663, 948
- Goerdt T., Moore B., Read J. I., Stadel J., Zemp M., 2006, MNRAS, 368, 1073

- Governato F., et al., 2009, preprint (astro-ph/0911.2237)  
Greco C., et al., 2007, ApJ, 670, 332  
Gualandris A., Merritt D., 2008, ApJ, 678, 780  
Hashimoto Y., Funato Y., Makino J., 2003, ApJ, 582, 196  
Hernandez X., Gilmore G., 1998, MNRAS, 297, 517  
Hernquist L., 1993, ApJ, 86, 389  
Inoue S., 2009, MNRAS, 397, 709  
Jiang I.-G., Binney J., 2000, MNRAS, 314, 468  
Kim H., Kim W.-T., Sánchez-Salcedo F. J., 2008, ApJ, 679, 33  
Li N., Chen D.-M., 2009, Res. Astron. Astrophys., 9, 1173  
Lotz J. M., Miller B. W., Ferguson H. C., 2004, ApJ, 613, 262  
Lynden-Bell D., Kalnajs A. J., 1972, MNRAS, 157, 1  
Mackey A. D., Gilmore G. F., 2003, MNRAS, 340, 175  
Makino J., 1991, PASJ, 43, 621  
Mashchenko S., Couchman H. M. P., Wadsley J., 2006, Nat, 442, 539  
Mashchenko S., Wadsley J., Couchman H. M. P., 2008, Sci, 319, 174  
Miller B. W., Lotz J. M., Ferguson H. C., Stiavelli M., Whitmore B. C., 1998, ApJ, 508, 133  
Miocchi P., Capuzzo-Dolcetta R., Di Matteo P., Vicari A., 2006, ApJ, 644, 940  
Navarro J. F., Frenk C. S., White S. D. M., 1997, ApJ, 490, 493  
Oh K. S., Lin D. N. C., Richer H. B., 2000, ApJ, 531, 727  
Ostriker E. C., 1999, ApJ, 513, 252  
Pesce E., Capuzzo-Dolcetta R., Vietri M., 1992, MNRAS, 254, 466  
Read J. I., Goerdt T., Moore B., pontzen A. P., Stadal J., 2006, MNRAS, 373, 1451  
Salucci P., Burkert A., 2000, ApJ, 537, 9  
Sánchez-Salcedo F. J., Reyes-Iturbide J., Hernandez X., 2006, MNRAS, 370, 1829  
Springel V., et al., 2008, MNRAS, 391, 1685  
Springel V., White D. M., 1999, MNRAS, 307, 162  
Strader J., Brodie J. P., Forbes D. A., Beasley M. A., Huchra J. P., 2003, AJ, 125, 1291  
Strigari L. E., Bullock J. S., Kaplinghat M., Simon J. D., Geha M., Willman B., Walker M. G., 2008, Nat, 454, 1096  
Tremaine S., 1976, ApJ, 203, 345  
Tremaine S., Weinberg M. D., 1984, MNRAS, 209, 729  
van Albada T. S., 1982, MNRAS, 201, 939  
Vesperini E., 2000, MNRAS, 318, 841  
Vesperini E., 2001, MNRAS, 322, 247